

Evidence of forcing of Arctic regional climates by mesoscale processes

P. Ola G. Persson¹ and R. Stone²,

¹ CIRES/NOAA/ESRL Physical Sciences Division, Boulder, Colorado USA

² CIRES/NOAA/ESRL Global Monitoring Division, Boulder, Colorado USA

1. SEARCH Observatories and Mesoclimates

Numerous environmental changes are currently being observed in the Arctic region, potentially impacting the Arctic and global climate systems and the people living in the Arctic. These changes include increases in the near-surface air temperature (e.g., Chapin et al 2005), decreases in the extent (e.g., Vinnikov et al 1999; Comiso 2002; Serreze et al 2003; Belchansky et al 2006) and thickness (Rothrock et al 1999) of the Arctic pack ice, and warming of Arctic permafrost and deepening of the soil active layer (e.g., Oelke et al 2004). While an increase in greenhouse gases is believed to be the overriding cause of these changes (IPCC 2001), the hypothesized mechanisms within the global climate system producing these specific changes can be broadly categorized into forcings by atmospheric dynamical, thermodynamic, and radiative processes; oceanic circulation and thermodynamic processes; and ice dynamics processes. To help monitor and better understand the causes for the changes being observed in the Arctic regions, the cross-disciplinary and multi-agency Study for Environmental Arctic Change (SEARCH; <http://www.arcus.org/SEARCH/index.php>) has been established (SEARCH, 2005).

To help address the objectives of SEARCH, the National Oceanic and Atmospheric Administration (NOAA), in collaboration with agencies in Canada and Europe, have formulated a plan to establish a few long-term, intensive, atmospheric observatories around the Arctic basin (Fig. 1). These intensive sites will provide "integrated time series measurements that include climate, surface energy balance, hydrology, glaciology, trace gases, permafrost/active layer, C/N/P budgets, species composition, vegetation structure, and contaminant compounds." (SEARCH, 2005, pg. viii). As many of the observed changes are in the near-surface environment, the surface energy budget (SEB) measurements are key.

To be able to utilize these new data sets to monitor and understand changes in the Arctic, the spatial representativity of these point data sets must be understood. Five of these SEARCH atmospheric observatories are located at Arctic coastal sites, and at least five of them would be considered to be located in complex terrain. Because such locations are known to frequently be strongly affected by local and/or mesoscale atmospheric processes, understanding the spatial representativity of the data being collected at the

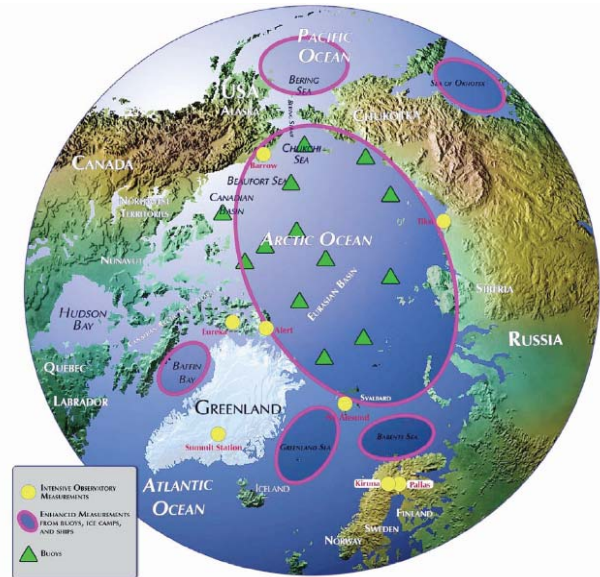


Fig. 1: Priority areas for atmospheric observation activities. A SEARCH Atmospheric Observing program should include coordinated intensive observatory measurements (yellow dots) in Barrow, Alaska; Alert and Eureka, Canada; Ny-Ålesund, Norway; Tiksi, Russia; the Greenland Summit Station; Pallas, Finland; and Kiruna, Sweden, as well as the inclusion of upper air measurements within existing ocean data collection activities (pink circles), including those from potential buoy deployment areas (green triangles). Weather station networks and satellite data (not shown) represent additional sources of atmospheric observations. (From SEARCH, 2005).

specific SEARCH sites becomes even more crucial. That is, the correlation length scales of atmospheric structures are typically quite short in such regions (e.g., Rigor et al 2000) which could be a significant problem for generalizing observed climate trends at these few Arctic sites to the entire Arctic region.

The issue of spatial representativity can be further understood if one considers the concept of mesoclimates, which are defined as "the climate of small areas of the earth's surface which may not be representative of the general climate of the district" (Glossary of Meteorology, 1995). Mesoclimates are generally produced by local or mesoscale (~10-200 km scale) processes, and can produce especially large gradients in temperature, wind, cloudiness (hence, surface radiation), precipitation, and snow cover in coastal regions and regions of complex terrain. That is,

in such regions, mesoclimates may vary significantly. Since these mesoclimates are forced by local or mesoscale processes, and the response of these smaller-scale processes to the various climate-change forcings are not well understood, it is uncertain whether trends measured at the few Arctic long-term observatories represent just the changes for the site's mesoclimate or whether the trends truly represent changes occurring over a larger region. For example, daily maximum near-surface air temperature trends in the Alaska region vary dramatically in magnitude, and even in sign, over relatively short distances (Fig. 2). Some coastal areas with complex terrain [e.g., (58°N, 136°W) and (61°N, 150°W)] have both negative and positive trends in close proximity, while the positive trends, which are in the majority, vary greatly in magnitude. The range of trends within this region is from -1.3°C/decade to +1.8°C/decade. Such variations may very well be explained by the presence of mesoclimates, and leads to the question whether different responses by mesoscale processes to climate forcing produce the observed large spatial variability in observed long-term trends?

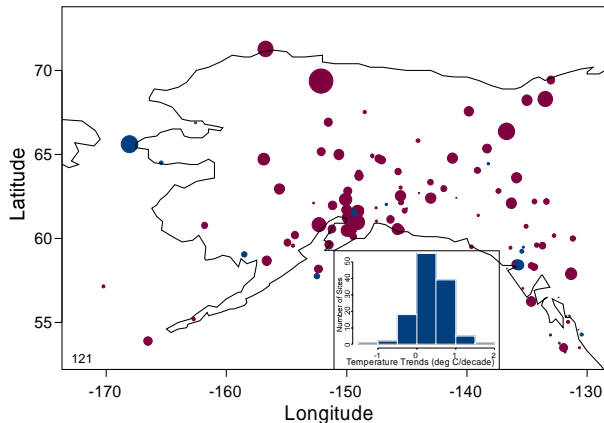


Fig. 2: Daily maximum near-surface temperature trends in the Alaska region since 1980. Blue dots show a negative trend and red dots a positive one; the size of the dot is proportional to the trend magnitude. The inset shows a trend histogram of the 121 sites. The data is from the National Climatic Data Center. (Courtesy of B. Weatherhead).

This paper will illustrate the near-surface mesoclimate at the Alert, Nunavut, SEARCH observatory site as revealed by the recently acquired surface energy budget data and analyses of the operational rawinsonde data. For context, aspects of the mesoclimate at Alert will be compared to those at the Barrow observatory site, located on a coastal plain, and to those at the 1997-1998 SHEBA site located on the pack ice in the Beaufort Sea, well away from coastal and terrain influences.

2. Alert Site Description

Alert is the furthest-north permanently inhabited location on earth at 82.5° N, 62.3° W (Fig. 3a). Surface and rawinsonde data has been collected since July, 1950, at the main military base (also referred to as Alert Canadian Forces Station - Alert CFS), located on a hill at 31 m above sea level near a bay of the Arctic Ocean. A large variety of additional data is being collected at the Global Atmospheric Watch (GAW) Laboratory located 7 km south of the military base in an elevated valley at 188 m MSL (Fig. 3b and Fig. 4b). The Alert region is a coastal region with complex terrain both locally and regionally, as local hills reach elevations in excess of 500 m and mountains within 100 km to the southwest of Alert reach elevations of 1500 m MSL.

Starting in August 2004, NOAA's Earth System Laboratory (formerly NOAA's Environmental Technology Laboratory and Climate Monitoring and Diagnostic Laboratory) installed instruments on a main scaffolding and a radiation mast near the Alert GAW Laboratory. On the main scaffolding, instruments measure broadband downwelling radiation, diffuse and direct radiation, standard meteorological parameters, virtual temperature and three-component wind speed at 20 Hz, soil temperature to a depth of 120 cm, and precipitation. Estimates of cloudiness can be obtained from an all-sky camera installed in August 2005, while direct measurements of sensible heat and momentum flux are available from the sonic anemometer installed in February 2006. Broadband upwelling radiation and the snow depth are measured at separate mast about 50 m from the scaffolding.

3. Alert Climatology and Flow Regimes

Figure 5 shows that the mean annual temperature at Alert CFS is about -18° C. The 54-year record shows a distinct cooling trend during 1951-1979. A modest warming trend has been present since, though with significant interannual variability (e.g., 2004 was the second coldest year on record). The seasonal trends (Fig. 6) show fairly uniform cooling for all seasons during 1951-1979, but significant warming during the autumn is the primary reason for the modest warming trend for the annual mean temperature during 1979-2005.

The annual temperature cycle (Fig. 7) shows temperatures at or above freezing during June, July, and August, and temperatures averaging near -30° C for four winter months. Figure 7 also shows that significant temperature differences exist between Alert CFS and Alert GAW, with the latter being 3-4° C colder during November through April. This difference is likely due to the 157 m elevation difference between

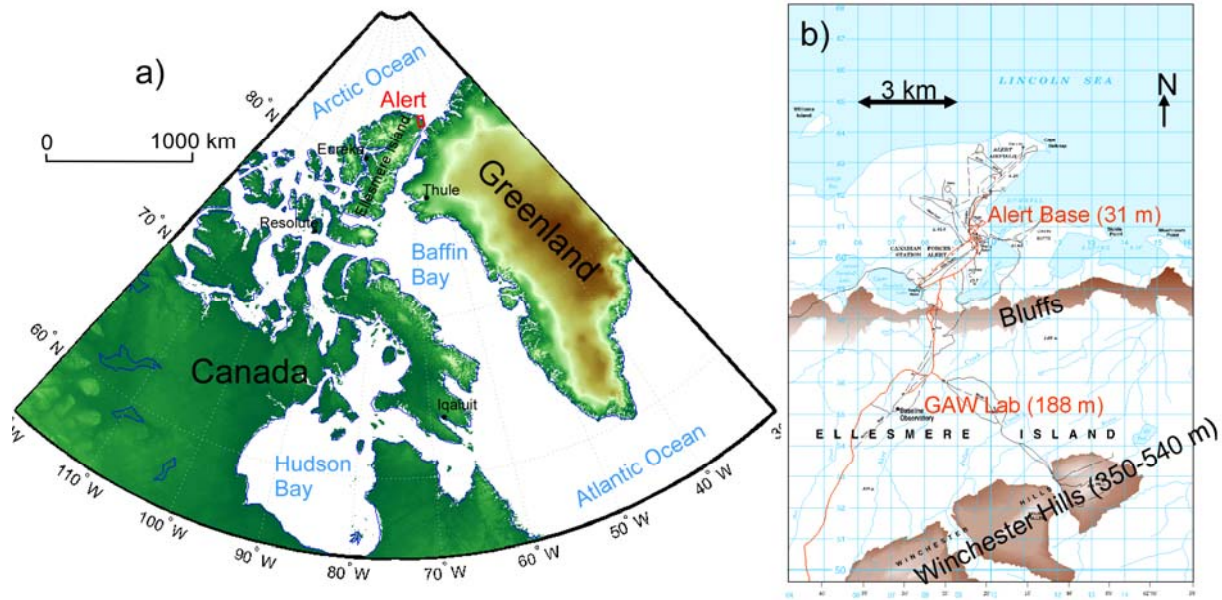


Fig. 3: Maps showing a) the location of Alert on Ellesmere Island in the Canadian Arctic and b) the local terrain, the long-term military base, and the Global Atmospheric Watch (GAW) station at Alert. The red rectangle in a) corresponds to the map area shown in b).

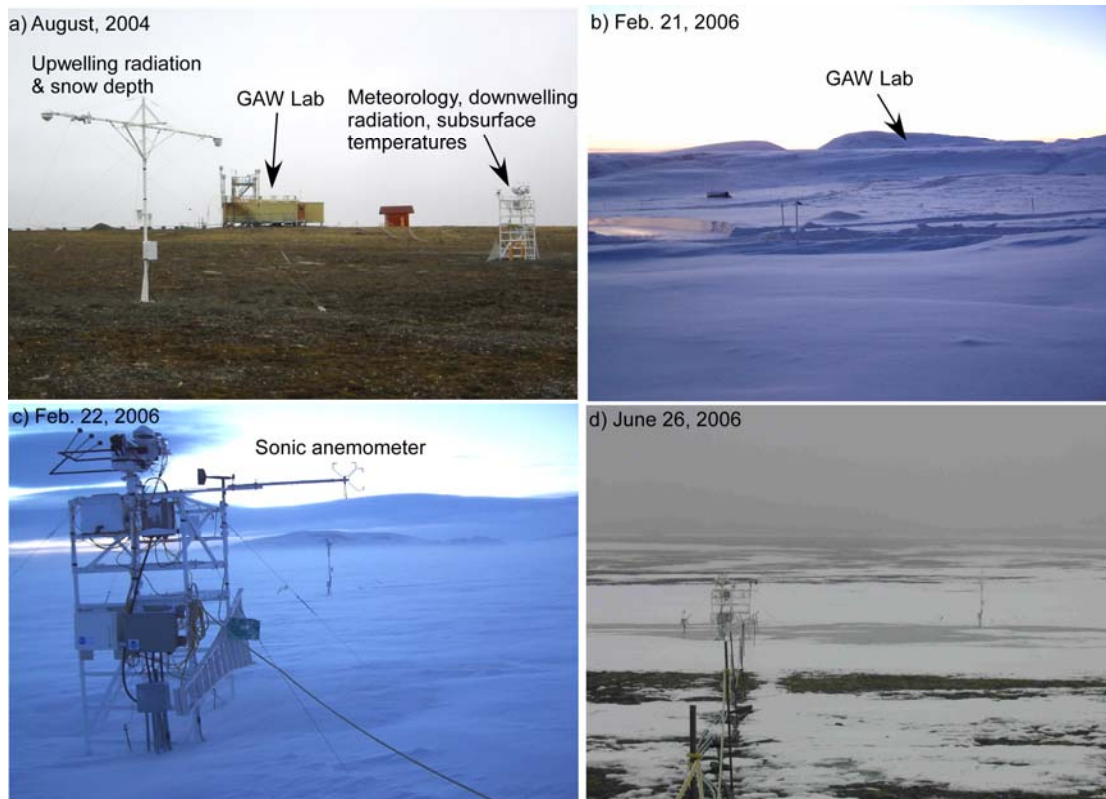


Fig. 4: Photographs showing a) the instruments near the GAW laboratory during a snow-free time of year, b) the location of the GAW laboratory as seen from the military base, c) the main instrument scaffolding and a blowing snow event during winter, and d) low clouds and fog during the snow-melt period (Photos by R. Stone (a), O. Persson (b & c), and J. Charlton (d)).

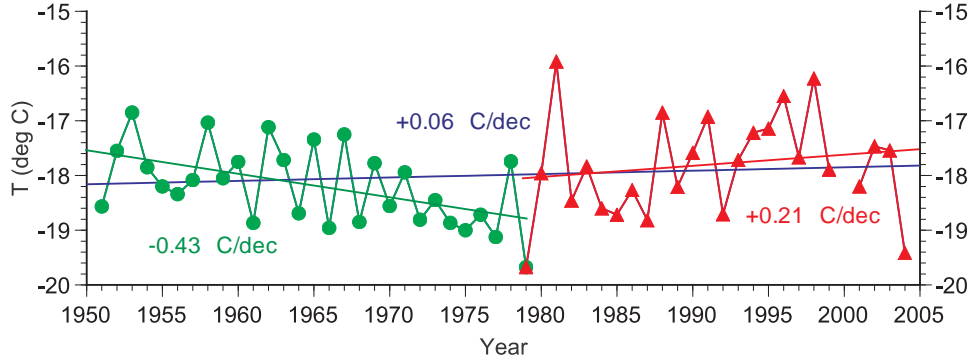


Fig. 5: Annual mean temperatures at Alert CFS from 1951 through 2005. The trends for the periods 1951-1979 (green; dots), 1979-2005 (red; triangles), and 1951-2005 (blue) are shown as straight lines. The mean trends (degrees Celsius per decade) for each period are also given and are color coded to the period (Data provided by Environment Canada at http://www.climate.weatheroffice.ec.gc.ca/climateData/canada_e.html).

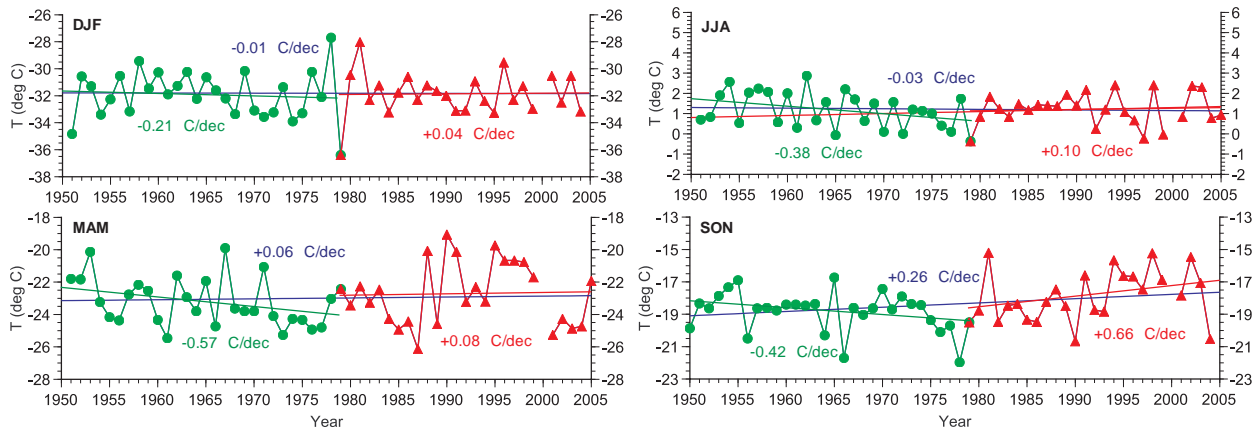


Fig. 6: As for Fig. 3 but for the seasonal means for winter (DJF), spring (MAM), summer (JJA), and autumn (SON).

the sites and the persistent, strong, low-level wintertime temperature inversion. Alert GAW is also about 1°C warmer than Alert CFS during July and August, when the snow has melted permitting above-freezing temperatures. To facilitate comparison, the monthly means in Fig. 7 use data from the same time period (8/2004-3/2006) for Alert GAW and Alert CFS. Figure 5 also compares the monthly mean temperatures at the Alert sites with temperatures at Barrow, a sea-level coastal site at lower latitudes (72°N) with no nearby significant topographic features, and with 3 data sets from pack ice stations. The wintertime Alert temperatures are colder than those at Barrow, but warmer than those over the pack ice, though Alert CFS only slightly so. The summertime temperatures at Barrow remain warm longer than at Alert, while those over the pack ice remain at or below freezing due to excess surface energy being used to melt sea ice rather than warm the surface (e.g., Persson et al. 2002).

Since the surface energy budget measurements are being made at the Alert GAW site, the wind data available from this site has been analyzed to identify

particular wind regimes. When the frequency of occurrence of all combinations of wind directions and wind speeds are computed, three, well-defined, narrow, wind regimes are clearly evident (Fig. 8). These are weak flow from the SW (wind speed $< 5\text{ m s}^{-1}$ and wind direction between 170° - 270°) occurring 47.5% of the time on an annual basis (Fig. 8a), weak flow from the NE (wind speed $< 7\text{ m s}^{-1}$ and wind direction between 30° - 110°) occurring 13.3% of the time, and strong flow from the SW (wind speed $> 5\text{ m s}^{-1}$ and wind direction between 180° - 250°) occurring 10.5% of the time. Examining how the wind regimes are distributed through the various seasons, the data shows that both SW wind regimes are more frequent during the winter (the plots for autumn and spring are very similar to the winter ones), while the NE flow regime is primarily a summer wind regime (Figs. 8b and 8c). Examining the topography in the upwind direction for each of these regimes shows that the SW regimes represent airflow from the higher interior of Ellesmere Island including the distant ice caps extending to over 1500 m (Fig. 8d) and from the direction of the Kane Basin and Kennedy

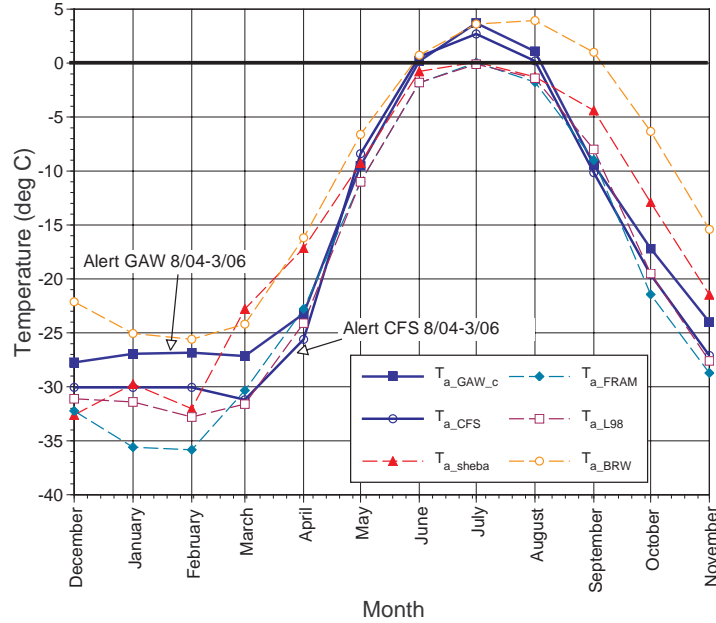


Fig. 7: Monthly mean near-surface air temperatures at Alert GAW (blue solid square), Alert CFS (blue open square), SHEBA (red triangle; Persson et al 2002), Nansen's 1893-1896 Fram expedition (cyan diamond; Mohn 1905), Russian drifting ice stations (purple open square; Lindsay 1998), and Barrow (gold open square)

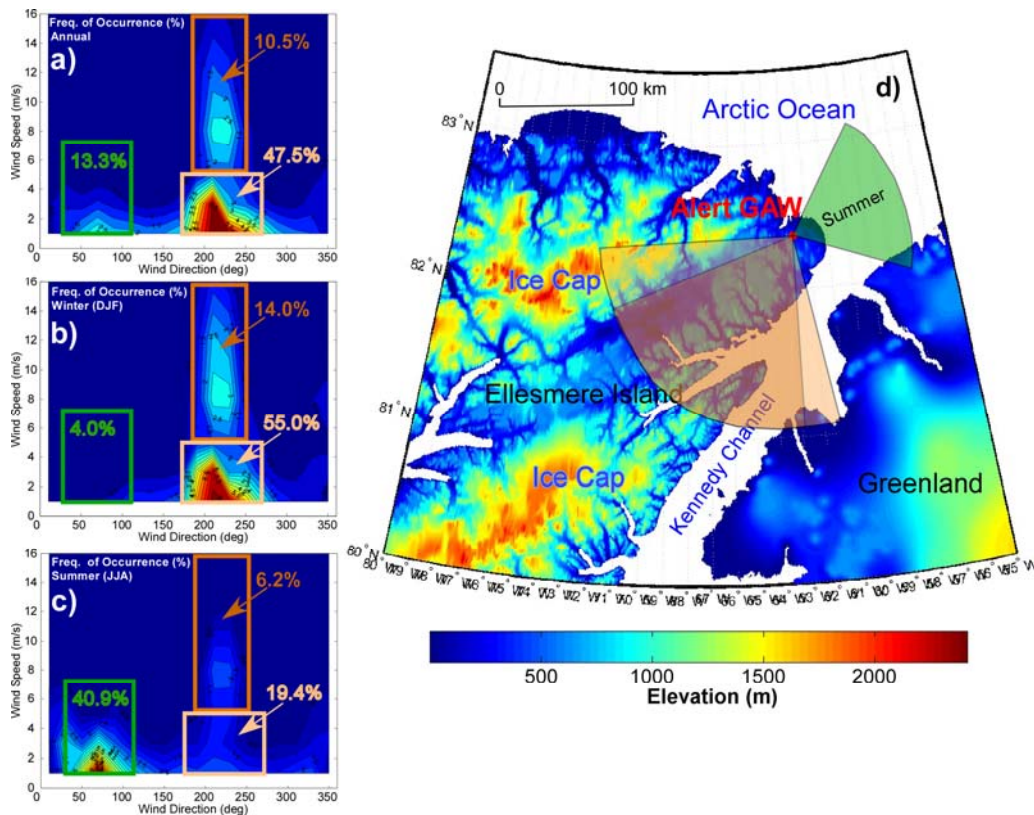


Fig. 8: Color coded isopleths of the frequency of occurrence of wind direction and wind speed combinations at Alert GAW for the a) entire year, b) winter (DJF), and c) summer (JJA). The boxes highlight the three main wind regimes (weak SW [tan], strong SW [brown], and summertime NE [green]) at the Alert GAW station. The total frequency of occurrence within each box is given. Data from 8/2004 through 3/2006 are used. Panel d) shows the upwind terrain for the three wind regimes.

Channel between Ellesmere Island and Greenland. Hence, these flow regimes represent downslope wind events. The summertime NE wind regime comes primarily from the ice-covered Arctic Ocean, and hence represents an onshore sea-breeze flow regime. Later analysis will show that this onshore flow is likely due to sea-land temperature contrasts that form once the inland snow cover has melted, and hence represents a "sea-breeze-like" wind regime.

These dominant wind regimes have distinctly different atmospheric characteristics. In general, the weak SW and NE air flows tend to be cold, while the strong SW air flow tends to average 3-5° C warmer (Fig. 9a). The relative humidity of the NE airflow tends to be highest, with the wintertime values of RH_{ice} averaging greater than 100% (Fig. 9b). The strong SW airflow tends to have the lowest relative humidity. However, the mixing ratio is not the lowest for the strong SW airflow (Fig. 9c). In fact, during the winter, the mixing ratio is highest during this regime. Hence, the strong SW airflow has low relative humidity but high temperatures and absolute humidity.

The physical process leading to these characteristics of the strong, downslope, SW wind regime is further suggested by examining time-height sections produced from rawinsonde data (Figs. 10 and 11). The vertical temperature structure of the Arctic atmosphere typically consists of the Arctic inversion (e.g., Kahl 1990), which typically has its top near 1 km MSL (Fig. 10a). However, significant undulations are

evident in the 12-day time-height section shown, and the frequency of these undulations (3 in 12 days) appear to be greater than that noted by Persson et al (1992) at Barrow and over the Beaufort Sea pack ice (2-3 times in 33 days). Clearly, additional studies of the characteristics of the Arctic inversion at Alert are warranted.

Using trough lines in the virtual potential temperature (θ_v) field (Fig. 10a), tongues of descending warm air can be seen, and many of these tongues are coincident with a sharp downward bend in the inversion-top height. These tongues suggest that air is descending in layers at least 2 km thick, and most of these layers are nearest the surface. The depressions of the inversion top suggest that the air descends between 0.5 km and 1.5 km. As the air descends, the potentially warmer air near the top of the inversion approaches the surface and warms.

Also note that a humidity inversion exists in the absolute humidity field (Fig. 10b) with a maximum near 1-2 km, and that air descending from the inversion top will bring higher absolute humidity towards the surface. Figure 10d shows that the relative humidity tends to decrease along the trough lines towards the surface, again supporting the notion that the air at the Alert GAW station during the strong SW wind regimes represents air that descends, and hence is warmed, but maintains its absolute humidity, thereby decreasing its relative humidity.

Figure 11, showing time-height sections of just the lowest 500 m of the atmosphere, shows that the strong winds are sometimes, but not always, coincident with the axes of maximum warming, that a substantial temperature difference can exist between the Alert GAW and the Alert CFS sites (up to 9° C in this cross-section), that the strong wind events don't always reach to the Alert CFS site, that significant directional shear often exists between the height of the CFS station and the GAW Lab, and that the RH_{ice} values during the weak wind regime at the GAW Lab height (YD 50-53) are supersaturated and significantly higher than at the Alert CFS station (YD 56.0) appears to not have a vertical link to heights above about 300 m, though this may just be an artifact of the 12-hour resolution of the rawinsondes.

3. Annual SEB at Alert GAW

The focus will be on understanding the processes modulating the surface energy budget (SEB) at the SEARCH sites. The SEB is expressed by

$$F_{tot} = SW_d - SW_u + LW_d - LW_u - H_s - H_l + C \quad (1a)$$

$$= SW_{net} + LW_{net} - H_{turb} + C \quad (1b)$$

$$= F_{atm} + C, \quad (1c)$$

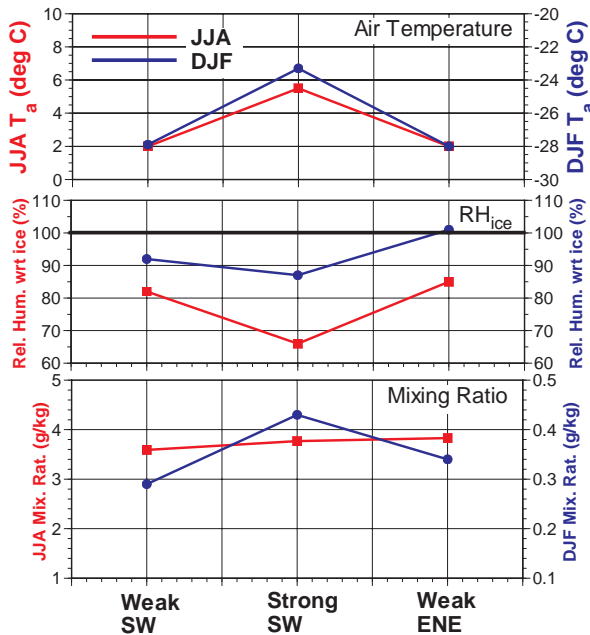


Fig. 9: Seasonal means of a) air temperature, b) relative humidity wrt ice, and c) mixing ratio for the three primary wind regimes at Alert GAW for summer (red) and winter (blue).

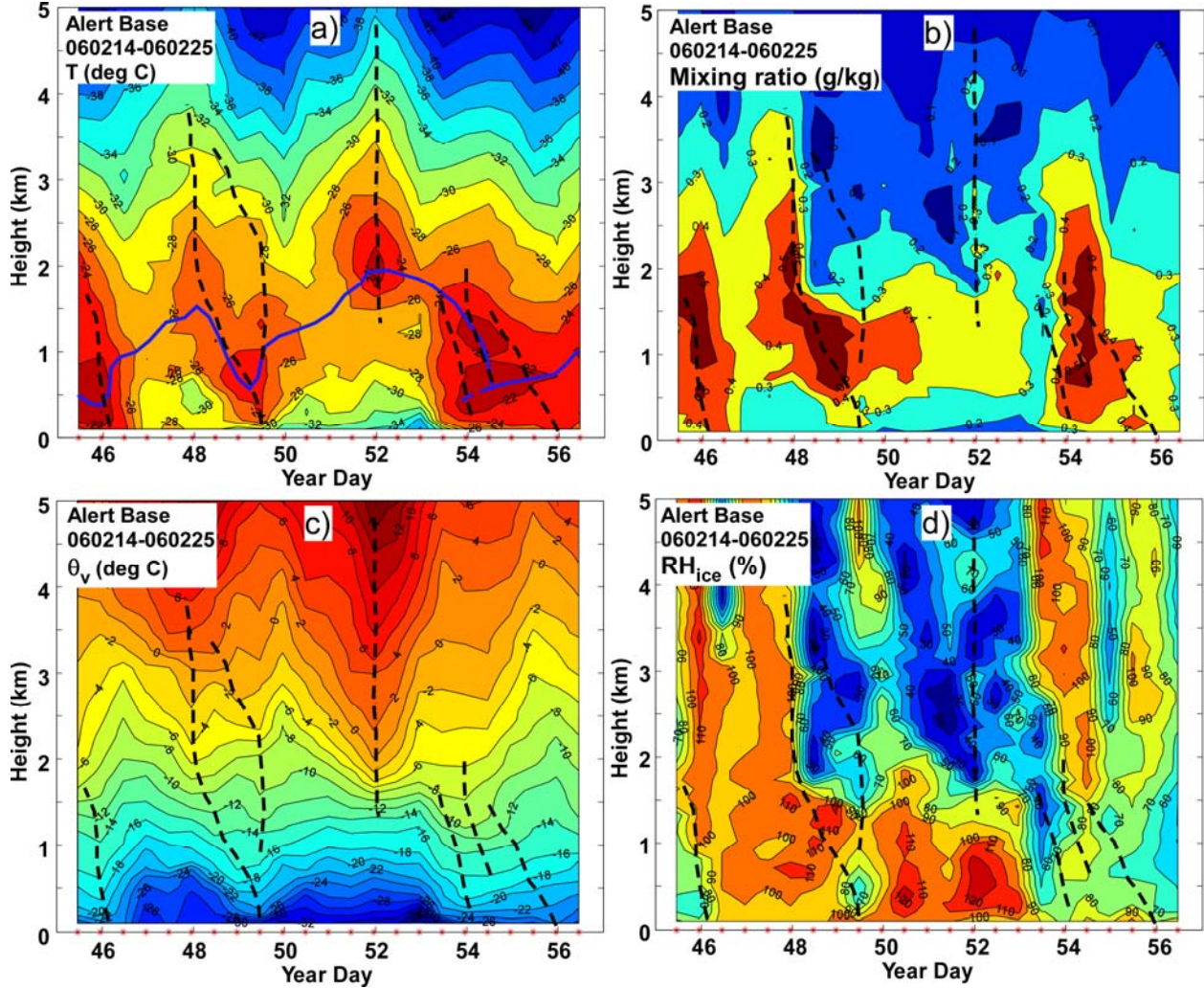


Fig. 10: Time-height sections of a) temperature, b) mixing ratio, c) virtual potential temperature (θ_v), and d) relative humidity with respect to ice from serial rawinsonde ascents at Alert CFS during Feb. 14-25, 2006 (YD 45-56). The erratic blue line in a) marks the top of the Arctic inversion, while the dashed lines in all panels mark locations of "trough lines" (warm axes) in the θ_v field. The red stars on the abscissa show the times of the rawinsonde launches.

where F_{tot} is the net surface energy flux; $F_{\text{atm}} = (SW_{\text{net}} + LW_{\text{net}} - H_{\text{turb}})$ is the atmospheric energy flux at the surface (snow, ice, or soil); SW_d , SW_u , LW_d , and LW_u are the incoming (downwelling) and outgoing (upwelling) shortwave and longwave radiative fluxes and $SW_u = \alpha SW_d$; H_s and H_l are the turbulent sensible and latent heat fluxes; C is the conductive flux in the soil or snow; and α is the surface albedo which varies with surface type, time of year, etc. In this study, all of the terms in (1) are measured except for H_s and H_l .

Though data to directly compute H_s has been obtained since February 2006, for the purposes of this study H_s and H_l are calculated using the bulk parameterization used for the SHEBA study (Persson et al. 2002). Hence, they are called H_{sb} and H_{lb} , respectively. Bulk fluxes were computed from specifications of 1-hr mean surface temperature, air

temperature, humidity, and wind speed. The surface specific humidity is obtained from the surface temperature, assuming ice-saturated conditions. A modified form of the Coupled Ocean Atmosphere Response Experiment (COARE) sea-air flux algorithm (Fairall et al., 1996) was used. A velocity roughness length (z_0) of 4.5×10^{-4} m was specified as used for SHEBA. Temperature and moisture roughnesses were taken from the snow-ice parameterization of Andreas (1987).

Monthly mean values of the various SEB terms are computed from hourly averages of the measurements for the time period August 2004 - March 2006. The annual cycle of these monthly means show that the net atmospheric energy flux (F_{atm}) is negative from September through April (Fig. 12a). That is, during 8 months of the year the combined effect of

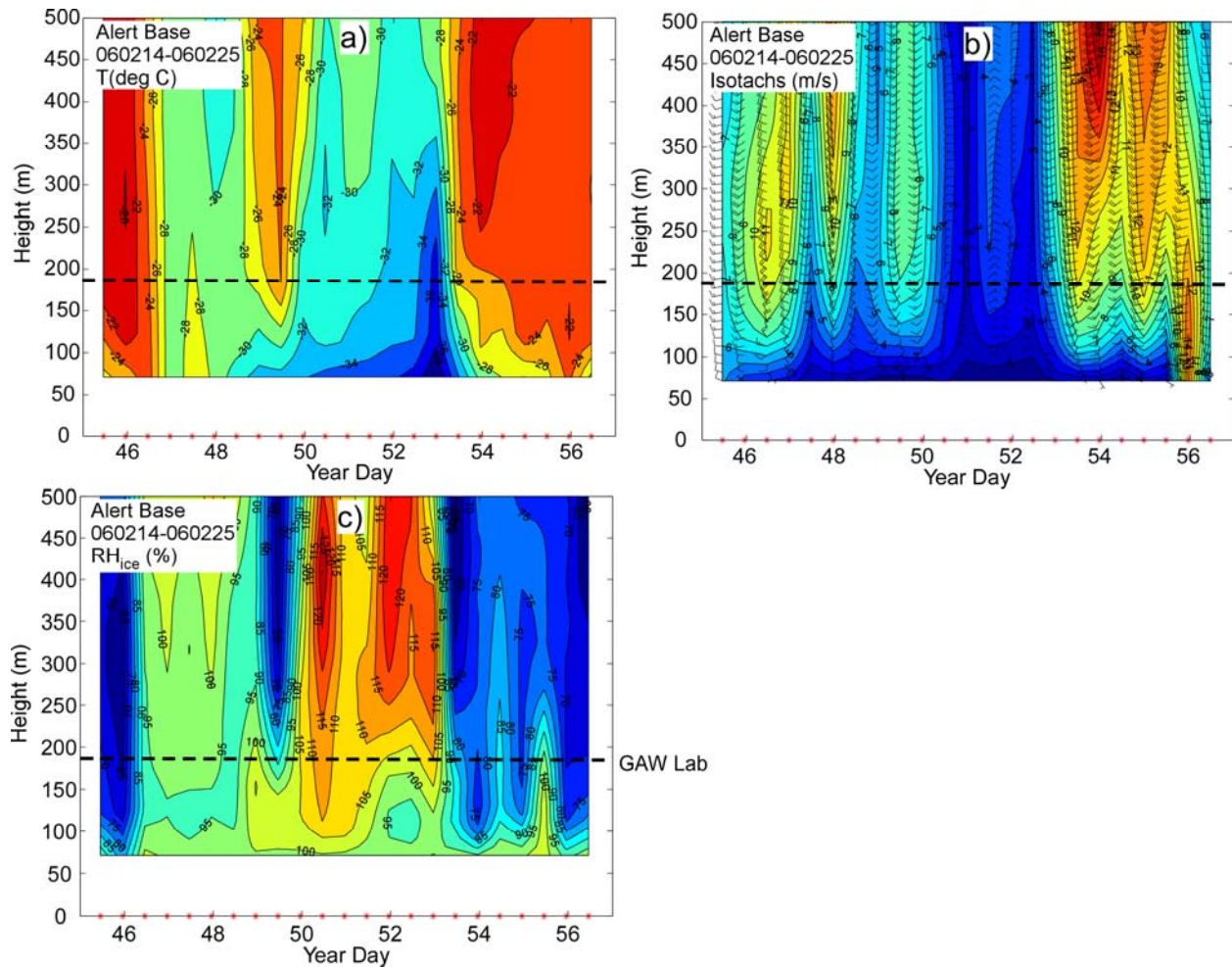


Fig. 11: Time-height sections from sea level to 500 m altitude of a) temperature, b) wind speed and wind flags, and c) relative humidity with respect to ice from serial rawinsonde ascents at Alert CFS during Feb. 14-25, 2006 (YD 45-56). The dashed black line marks the height of the Alert GAW station. The red stars on the abscissa show the times of the rawinsonde launches.

radiative and turbulent processes produces a net energy loss of $5\text{-}20 \text{ W m}^{-2}$ per month at the surface, which is generally snow covered during this time period. However, during May through August, the surface gains energy, with a maximum gain of about 80 W m^{-2} occurring in June. During the year, the surface gains about 2.8 W m^{-2} . Some of this energy gain is used to melt the snowpack, which melts entirely during the summer (typically by late June/early July-- see Fig. 4d).

The melting of the snowpack of about 0.40 m depth with a density of 350 kg m^{-3} requires an annual average energy flux of about 1.49 W m^{-2} . Hence, during the 19-month data period, the annual energy flux excess at Alert GAW is about 1.31 W m^{-2} (i.e., $2.8 \text{ W m}^{-2} - 1.49 \text{ W m}^{-2}$). This excess energy flux is equivalent to the energy required to melt 0.14 m of ice, and likely is used to melt the permafrost and increase the depth of the soil active layer.

Since no "tuning" of the above calculations have been done, many uncertainties exist in this calculation. Hence, it should only be considered as a preliminary estimate, but it does illustrate the small magnitudes of the important annual average energy fluxes. Uncertainties exist in both the terms that have been parameterized (H_{sb} and H_{lb}) and those that are directly observed (SW_{net} , LW_{net}). All of these terms are seen to be important during at least part of the year (i.e., have monthly mean magnitudes significantly greater than the annual average F_{atm}). For instance, significant cooling is produced by H_{lb} , H_{sb} , and LW_{net} during the summer, which offsets the strong warming by SW_{net} due to the low albedo once the snow is melted. Clearly, the parameterizations for the turbulent energy fluxes need to be verified with direct covariance measurements of these fluxes to ascertain that no significant bias (i.e., one of 1 W m^{-2} or greater) exists. If significant turbulent energy fluxes are produced by

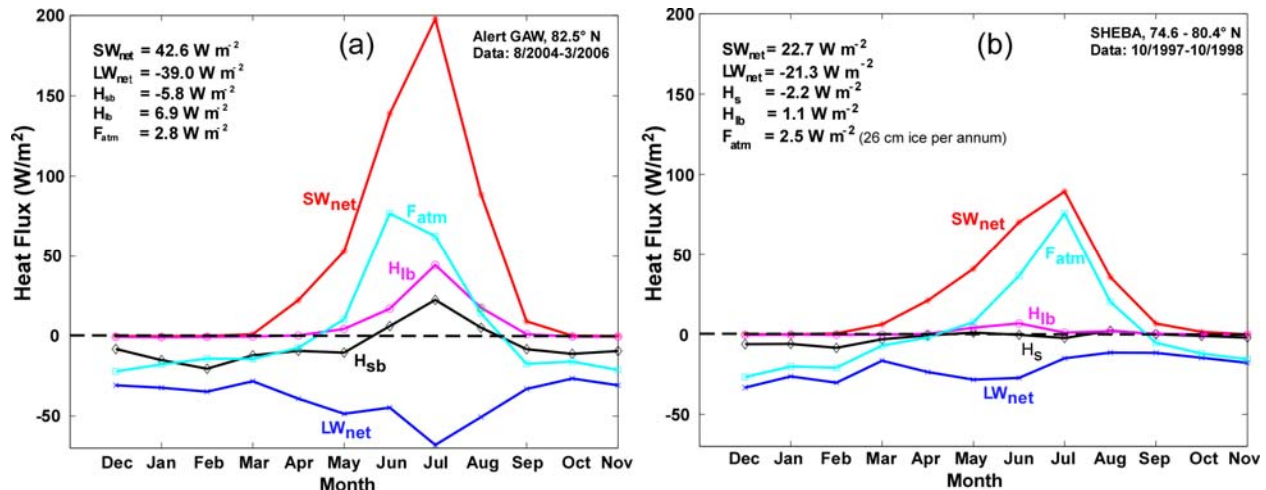


Fig. 12: Annual cycle of the various terms of the SEB at a) Alert GAW and b) SHEBA. The annual mean values of the terms are shown in the upper left of each panel.

non-Monin-Obhukov Similarity Theory processes (e.g., gravity waves), or are present in the very stable conditions that sometimes exist, the flux parameterization scheme used is not adequate. The sonic anemometer data currently being collected at Alert GAW will be used to address these concerns, and new schemes such as those developed by Grachev et al (2006) will be tested. Similarly, the net radiative fluxes, which are the difference between very large incoming and outgoing radiative fluxes, were estimated to have biases of -6 – 0 W m^{-2} for SW_{net} and ± 4 W m^{-2} for LW_{net} during SHEBA (Persson et al 2002). A complete error analysis of the Alert GAW data set will not be attempted here but is necessary in the future.

A similar analysis of the SEB on the pack ice at SHEBA (October 1997–October 1998) provides an interesting comparison to that at the Alert GAW terrestrial site (Fig. 12b). The annual mean F_{atm} was 2.5 W m^{-2} during that year, almost identical to that observed at Alert GAW. This energy excess is equivalent to that needed to melt about 0.26 m of ice, and hence accounts for 74% of the net ice loss (including snow melt) observed at SHEBA. However, the magnitudes of all of the individual terms are much smaller over the pack ice. The summertime SW_{net} is much smaller because the albedo of the ice is much greater than that of the land after the snow cover melts, while the summertime LW_{net} is less negative because the surface temperature over the ice pack remains at 0° C. The smaller summertime magnitudes of H_{sb} and H_{lb} are likely also caused by the colder surface temperatures at SHEBA, while the warmer wintertime surface temperatures at SHEBA (see Fig. 7) may produce weaker downward H_{sb} over the pack ice. However, terrain-induced mesoscale processes may also be affecting the radiative and turbulent terms at the Alert GAW site, as will be discussed below.

The hourly energy fluxes were subsampled according to whether they occurred in association with one of the main three wind regimes described in section 3. Figure 13 summarizes the seasonal-mean SEB terms classified by wind regime. During the winter (Fig. 13a), which is similar to the autumn and spring seasons, the greatest radiative loss is for the SW wind flow, especially the strong SW wind flow, because of the fairly low LW_d and the very low LW_u (large in magnitude). The large magnitude of LW_u results from the relatively warm surface temperatures during the strong SW regime. However, the strong SW wind regime also produces the least net energy loss (F_{atm}) because of the very strong turbulent energy transfer (~ 43 W m^{-2}) to the surface by H_{sb} . The greatest net energy loss occurs for the weak SW wind regime, which is also the most frequent regime (55%), as the H_{sb} for this regime is much less.

The summertime SEB is more complicated. As in the winter, clear skies (low LW_d , high SW_d) predominate for the strong SW winds (Fig. 13b). However, the lower albedo occurring after the snow has melted, which is the primary time of occurrence of the weak ENE wind regime, produces the maxima in SW_{net} and Q_{net} ($= \text{SW}_{\text{net}} + \text{LW}_{\text{net}}$) for the ENE wind regime. (The late-summer predominance of the ENE wind regime after the disappearance of the snow cover suggests that a sea-breeze type of processes is the primary mechanism of the ENE wind regime.) The strong Q_{net} for the ENE regime is partially offset by turbulent cooling through both H_{sb} and H_{lb} , while turbulent warming through H_{sb} offsets the turbulent cooling through H_{lb} for the strong SW winds. The net effect is that the strongest summertime heating is produced during the strong SW wind regime, with again H_{sb} being a crucial flux differentiating the regimes.

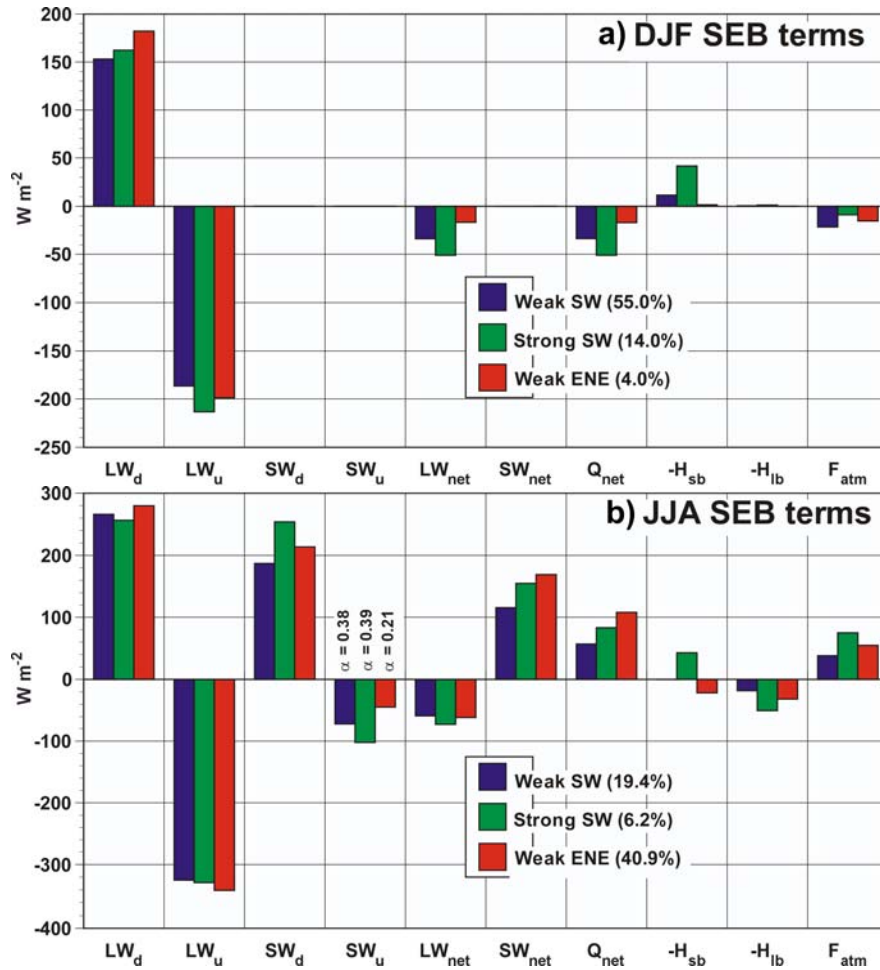


Fig. 13: The seasonal means of the SEB terms at Alert GAW broken up into the three wind regimes and summarized in bar graphs for a) winter (DJF) and b) summer (JJA). The percentages shown by the wind regime legends indicate the frequency of occurrence of each regime for the indicated time period. The mean surface albedos for SW_u in b) are also given.

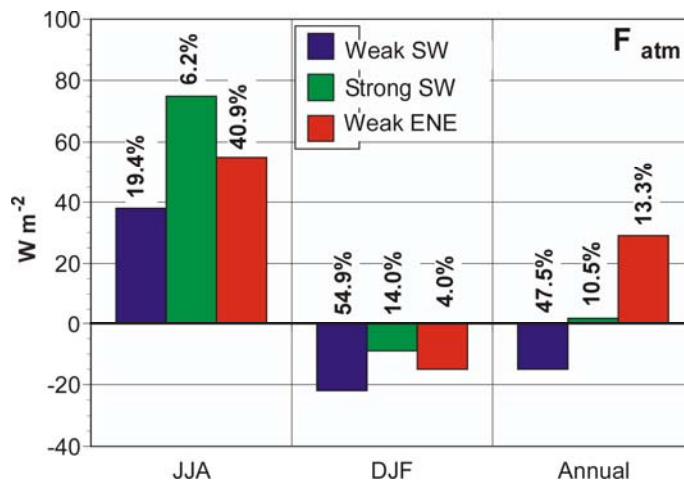


Fig. 14: The values of F_{atm} for summer, winter, and the whole year. The percentages shown each bar indicate the frequency of occurrence of each regime for the indicated time period.

Hence, examining the net atmospheric flux (F_{atm} ; Fig. 14) shows that the strong SW wind regime produces the least cooling in winter and the strongest warming in summer. However, the ENE wind regime produces the greatest F_{atm} on an annual basis because it occurs primarily in the summertime when all the wind regimes are associated with positive F_{atm} . Clearly, the strong SW wind regime is important to the SEB of the Alert GAW site throughout the year while the weak ENE wind regime is important during the summer. Both of these wind regimes are likely caused by mesoscale processes, the first associated with the presence of the complex terrain and the latter resulting from the proximity of a coastline.

4. Discussion of Links Between Mesoscale Processes and Climate

Coastal regions are known to generate mesoscale circulations and local climatic regimes because of processes resulting from differential friction, differential heating, and differential moisture supplies. Differential frictional effects can cause coastal convergence of boundary layer flows, thereby producing enhanced upward motion and clouds in these regions. These clouds can be enhanced by the direct moisture supply from the ocean, an effect which can also occur in the Arctic as regions of open water polynyas and fast-ice fracture leads frequently occur near the coastlines, such as near Barrow.

Outside of polar regions, differential heating and cooling near coastlines are known to cause sea and land breezes, respectively. Once the snow has melted in the Arctic summer, significant temperature differences between ice-covered oceans and land regions occur and cause sea breezes there as well (Moritz 1977; Kozo 1982a,b). In the high Arctic, temperatures over land are typically near 5°C in July and August and can frequently reach 15°C , while the ice-covered ocean never goes above 0°C . The stronger Coriolis force, the greater stability, the shallower boundary-layer depth, and the weak diurnal cycle creates sea-breeze circulations that differ from those at lower latitudes (e.g., Kozo 1982b). At high latitudes, the sea-breeze circulation is in phase with the diurnal heating and will be confined to a distance $Nh(f^2 - \omega^2)^{-0.5}$ of the coastline, where N^2 is the Brunt-Väisala frequency, h is the heating depth, f is the Coriolis parameter, and ω is the rotation frequency of the earth (Rotunno 1983). For reasonable values of h (200 m) and N ($2 \times 10^{-2} \text{ s}^{-1}$) at Alert (latitude = 82.5°N), the circulation will be confined to within 32 km of the coast. Because the stronger Coriolis force and shallower heating depths in the Arctic are only partially compensated by the greater stability, this value is about

a factor 5 smaller than at mid-latitudes. Its relatively small value suggests that coastal long-term sites may only represent a narrow region along the Arctic coast.

While land breezes may not occur frequently in the Arctic summer since the land will frequently not cool below the temperature of the adjacent ocean because of the continued solar forcing during the Arctic summer “nights” (Kozo 1982b), terrestrial sites in the Arctic may experience stronger wintertime cooling than the oceanic locations, thereby conceivably producing wintertime land breezes. Long-term wind roses from Arctic coastal sites clearly show prevalent onshore flow in July when the snow has melted and offshore flow through most of the winter months.

Sea (land) breezes establish a circulation, transport cooler air inland (offshore), and may alter the cloudiness. These effects can all impact the surface energy budget of a coastal site through their effects on the sensible and latent turbulent heat fluxes and radiative fluxes. Haugen and Brown (1980) noted that Atqasuk, located 48 km south of the Beaufort Sea coastline in northern Alaska, had a mean July temperature of 8.7°C compared to that for Barrow right at the coast of 3.7°C . Furthermore, they also noted that the inland temperature increase was directly related to the distance from the coast along the mean 75° wind direction rather than on the nearest distance to the coast, suggesting that a significant sea breeze affected the near-coast July temperatures. Also, trace precipitation amounts occurred more frequently at Barrow than inland, again suggesting a coastal effect on clouds and drizzle occurrence.

If steep topography also occurs near a coastline, the mesoscale effects can become much more complex. Regional topographic lifting of low-level flow can produce enhanced cloudiness and precipitation, the former affecting the surface radiation and the latter affecting the annual cycle of the surface albedo (and hence the net surface radiation) as well as the conductivity flux into the surface. Interactions between topography and the large-scale or synoptic-scale flow can also lead to katabatic wind events (such as those observed in Antarctica), either being of a foehn (warm) or bora (cold) nature. Foehn events are generally accompanied by clear skies, strong winds, and relatively warm air, all of which have significant effects on the surface energy budget. The analysis from the Alert SEARCH site in sections 2 and 3 suggests that foehn-like events produce the least surface cooling in the winter and the greatest surface warming in the summer, primarily because of the very large downward (into the surface) turbulent sensible heat flux accompanying these events. An analysis of 6 years of twice-daily sounding data from the complex Eureka site

on the shore of the Slidre Fjord suggests that a combination of sea-breeze effects, topographic channeling, and katabatic flows may be occurring.

Another obvious impact of topography on the mesoclimate of a site is the direct effect of a site's altitude on its temperature. However, in contrast to the mid-latitudes, increased altitude in the Arctic region generally leads to a warmer climate because of the pervasive Arctic inversion, especially during the winter. The wintertime Arctic inversion may be as strong as 10°C or more in the lowest 1000-1500 m (e.g., Figs. 10 and 11), and this inversion strength may vary depending on the processes producing the local inversion. Therefore, a site that is at only 200 m above sea level may easily have a mean annual temperature that is 2°C warmer than a site at sea level. Much of the area in the vicinity of both Eureka and Alert are 100-300 m above the long-term stations, which are near sea level. In addition, clouds often form at heights below 500 m in the Arctic, and sometimes below 100 m. Hence, the cloud climatology can also be very dependent on the site elevation, in addition to its dependence on the proximity of the coastline and the effects of topographic lifting or subsidence. The generally large stability and shallow boundary layers in the Arctic mean that a site's climatology is even more sensitive to altitude than at mid-latitude sites.

Ralph et al (2003) present a useful example illustrating how local terrain and coastline effects may alter the interpretation of data from long-term sites. Two central California watersheds have weaker floods during strong El Niño events than during non-El Niño years, which contrasts with the general occurrence of stronger floods during these events at nearby watersheds. Ralph et al (2003) showed that the predominant wind direction during flooding events for the El Niño regimes were more southerly by about 14 degrees compared to those for non-El Niño years. This subtle change in the predominant airflow placed these two watersheds in the lee of higher portions of coastal topography during the El Niño years, thereby leading to less intense precipitation and weaker floods. Thus, the interpretation of El Niño effects on these local watersheds was altered. As storm tracks and storm intensities change in response to Arctic warming (e.g., Knippertz et al 2000; Pinto et al 2006), shifts in predominant wind directions are likely to occur (along with changes in other parameters). These shifts can produce changes in the cloudiness, frequency of downslope wind storms, snowfall, etc.

Similarly, many mesoscale phenomena are modulated by the characteristics of the larger scale, typically synoptic-scale, flows. For instance, it is well known that the sea-breeze strength and effect in mid-latitudes is greatly modulated by the coast-perpendicular component of the geostrophic wind and

the land-sea temperature gradient. Miller and Keim (2003) show that sea breezes can form along the New England coast for land-sea air temperature differences of 5-10°C with an offshore geostrophic wind of up to 5-8 m s⁻¹, but stronger offshore geostrophic winds inhibit their formation. Kozo (1982b) showed that a weak offshore large-scale flow inhibited the inland penetration of the sea breeze along the Beaufort Sea coastline, while onshore flow strengthened the sea breeze flow. Downslope wind events are dependent on the wind direction relative to the topography, the height of the topography, and the stability structure of the large-scale flow (e.g., Smith 1985; Durran 1986). These dependencies present the possibility that changes in the frequency of occurrence of the mesoscale processes resulting from changes in the large-scale or synoptic flow direction or stability characteristics can produce local changes to the surface energy budget that may or may not be representative of the larger-scale changes. It is not yet known how the large-scale and synoptic-scale flow in the Arctic might change in the future; however, it is clear that changes are very possible, so the frequency and/or intensity of the mesoscale or local-scale processes are likely to change because of their modulation by the changing synoptic scale.

Our primary hypothesis is that many mesoscale or local scale processes, some of which are discussed above, occur near the SEARCH sites because of their proximity to coastlines and complex terrain in an environment that is typically highly stratified. If they do occur, this raises the question whether the observed climatology and climatological changes at the SEARCH long-term sites represent only very local areas or whether they represent a larger regional or even Arctic domain. That is, if the atmospheric processes producing the mesoclimate of the SEARCH sites are the processes dominant in the region, then it is likely that climatological changes to the forcing of those processes will produce changes to the mesoclimate at the SEARCH sites that are representative of the changes in the region. However, if the mesoclimate at the SEARCH site is produced by processes that only occur locally within the region, then the long-term changes at the SEARCH site may not represent the long-term changes in the region. Local changes at the SEARCH sites may even have the opposite sign to the regional changes, as in the example from the California coast discussed above or at some of the sites in Fig. 2.

5. Conclusions

The above discussion suggests that mesoscale processes likely impact many of the current and proposed long-term SEARCH observatories, producing mesoclimates at these sites. The detailed analysis of data from the Alert GAW laboratory shows that

mesoscale processes strongly impact the surface energy budget. Year-round, strong downslope wind events and summertime sea-breeze events modulate the annual SEB at this high-Arctic coastal site in complex terrain. Furthermore, the analysis has shown that the SEB annual cycle at this terrestrial site is significantly different than that observed on the pack ice far distant from any coastal or topographic effects during the SHEBA year. However, it is unclear whether the SEB differences between the sites are primarily due to the dominance of mesoscale processes at the terrestrial site or whether it is primarily due to the difference between ice and land as the surface medium. A quantitative separation of these effects is necessary to make this assessment. Such a separation is likely difficult, and has as yet not been done.

As the analysis at Alert GAW has shown, terrain-induced and coastline-induced mesoscale processes are likely to be important for the SEB at all SEARCH observatory sites. The presence of these mesoscale processes has two main effects. First, since these processes may have strong spatial variability, a strong spatial variability in the SEB may exist near the SEARCH observatory sites. Secondly, because the mesoscale processes are forced by specific atmospheric or surface characteristics, such as the airflow over a mountain range or the date of the disappearance of the terrestrial snow cover rather than temperature (the classical climate-change parameter), the climate and SEB at a specific site may respond differently to a changing large-scale climate than does the larger region as a whole. For instance, climate change may produce a change in the large-scale wind direction or in the wintertime precipitation amount. Such changes could produce changes in the relative frequency of the mesoscale processes shown to occur at Alert (e.g., more frequent strong SW wind events or a longer period of predominant summertime onshore flow events), which in turn could have a dominant impact on the response of the local total SEB to the climate change. These results suggest that the future climate change at the terrestrial sites will depend on the response of the dominant mesoscale processes to the large-scale Arctic changes, and may therefore not be of the same magnitude, nor sign, as the large-scale changes.

Acknowledgements

We greatly appreciate the efforts of the NOAA/ESRL technical staff for designing, deploying, and maintaining the instrumentation at the Alert GAW Laboratory, the latter sometimes occurring in difficult environmental conditions. We also appreciate the efforts of the Environment Canada staff in both Toronto and Alert for facilitating the establishment of the GAW site, providing real-time maintenance of the instruments, and facilitating the data transmissions. The

Alert CFS military personnel provided logistical support during deployment of the instrumentation. John Kivisto, the Environment Canada meteorologist in charge at Alert, provided interesting and useful discussions concerning the meteorological characteristics near Alert and provided us with the Alert CFS data from February 2006. Data processing assistance was provided by Amit Halevi and Amber Beutler. Financial support for SEARCH research at NOAA/ESRL is provided by NOAA/SEARCH research funds.

6. References

- Andreas, E. L., 1987: A theory for the scalar roughness and the scalar transfer coefficients over snow and sea ice, *Bound.-Layer Meteorol.*, **38**, 159-184.
- Belchansky, G., V. Eremeev, I. Mordvintsev, N. Platonov, and D. Douglas, 2006: Evolution, spatial, and inter-annual variability and trends in the Arctic's sea ice extent, age, and thickness distributions, 1979-2005. *Abstracts and Poster Presentation, European Geophysical Union Meeting*, Vienna, Austria, April 2-7.
- Bramwell, Martyn, 1979: *Rand McNally Atlas of the Oceans*. United States National Oceanic and Atmospheric Administration. Atlantic Oceanographic and Meteorological Labs., Miami, FL., Collected reprints, 1978, Boulder, CO., Dec., 1979. 24 pp.
- Chapin, F. S. III, M. Sturm, M. C. Serreze, J. P. McFadden, J. R. Key, A. H. Lloyd, A. D. MvGuire, T. S. Rupp, A. H. Lynch, J. P. Schimel, J. Beringer, W. L. Chapman, H. E. Epstein, E. S. Euskirchen, L. D. Hinzman, G. Jia, C.-L. Ping, K. D. Tape, C.D.C. Thompson, D. A. Walker, and J. M. Welker, 2005: Role of Land-Surface Changes in Arctic Summer Warming. *Science (Wash.)*, **310** (5748), pp. 657-660, 28 Oct 2005.
- Comiso, J. C., 2002: A rapidly declining perennial sea ice cover in the Arctic, *Geophys. Res. Lett.*, **29**(20), 1956, doi:10.1029/2002GL015650.
- Durran, D. R., 1986: Another look at downslope windstorms. Part I: The development of analogs to supercritical flow in an infinitely deep, continuously stratified fluid. *J. Atmos. Sci.*, **43** (21), 2527-2543.
- Fairall, C. W., E. F. Bradley, D. P. Rogers, J. B. Edson, and G. S. Young, 1996: Bulk parameterization of air-sea fluxes for Tropical Ocean-Global Atmosphere Coupled-Ocean Atmosphere Response Experiment, *J. Geophys. Res.*, **101**, 3747-3764.

- Haugen, R. K., and J. Brown, 1980: Coastal-inland distributions of summer air temperature and precipitation in northern Alaska. *Arctic and Alpine Research*, **12**(4), 403-412.
- Grachev, A. A., E. L. Andreas, C. W. Fairall, P. S. Guest, and P. O. G. Persson, 2006: The SHEBA profile functions in the stable atmospheric boundary layer. *Boundary-Layer Meteorol.*, in review.
- International Panel on Climate Change (IPCC): Climate Change 2001: *Synthesis Report, Summary for Policy Makers*. [Available at <http://www.ipcc.ch/pub/un/syrenseng/spm.pdf>]
- Knippertz, P., U. Ulbrich, and P. Speth, 2000: Changing cyclones and surface wind speeds over the North Atlantic and Europe in a transient GHG experiment. *Clim. Res.*, **15**(2), 109-122.
- Kahl, J. D., 1990: Characteristics of the low-level temperature inversion along the Alaskan arctic coast. *Int. J. Climatol.*, **10**, 537-548.
- Kozo, T., 1982a: An observational study of sea breezes along the Alaskan Beaufort Sea coast: Part I. *J. Appl. Meteorol.*, **21**, 891-905.
- Kozo, T., 1982b: A mathematical model of sea breezes along the Alaskan Beaufort Sea Coast: Part II. *J. Appl. Meteorol.*, **21**, 906-924.
- Lindsay, R. W., Temporal variability of the energy balance of thick Arctic pack ice, *J. Clim.*, **11**, 313-333, 1998.
- Miller, S. T. K., and B. D. Keim, 2003: Synoptic-Scale Controls on the Sea Breeze of the Central New England Coast. *Weather and Forecasting*, **18**, 236-248.
- Mohn, H., *The Norwegian North Polar Expedition 1893-1896, Scientific Results*, Volume VI, Meteorology, edited by F. Nansen, F. Nansen Fund for Advancement of Science, Christiania (Oslo), 1905.
- Moritz, Richard E., 1977: On a possible sea breeze circulation near Barrow, Alaska. *Arctic and Alpine Research*, **9** (4), 427-431.
- Oelke, C., T. Zhang, and M. C. Serreze, 2004: Modeling evidence for recent warming of the Arctic soil thermal regime. *Geophys. Res. Lett.*, **31** (7), L07208, doi:10.1029/2003GL019300.
- Persson, P. Ola G., D. Ruffieux, and K. Davidson, 1992: Characteristics of the lower troposphere during LeadEx 92. *Preprints, Third Conference Polar Meteorology and Oceanography*, 29 Sept - 2 Oct, 1992, Portland, OR, 50-53.
- Persson, P. Ola G., C. W. Fairall, E. L. Andreas, P. S. Guest, and D. K. Perovich, 2002: Measurements near the Atmospheric Surface Flux Group tower at SHEBA: Near-surface conditions and surface energy budget. *J. Geophys. Res.* **107**(C10), 8045, doi:10.1029/2000JC000705.
- Persson, O., R. Stone, M. Shupe, and T. Uttal, 2006: Investigating interactions of surface energy budget, boundary layer structure, and synoptic/orographic influences at climate monitoring observatories for the Study of Environmental Arctic Change (SEARCH). *Abstracts, European Geophysical Union Meeting*, Vienna, Austria, April 2-7
- Pinto, J. G., T. Spanghel, U. Ulbrich, and P. Speth, 2006: Comparing cyclone core pressure and vorticity changes in a transient greenhouse gas scenario. *Abstracts and Poster Presentation, European Geophysical Union Meeting*, Vienna, Austria, April 2-7.
- Ralph, F. M., P. J. Neiman, D. E. Kingsmill, P. O. G. Persson, A. B. White, E. T. Strem, E. D. Andrews, and R. C. Antweiler, 2003. The impact of a prominent rain shadow on flooding in California's Santa Cruz Mountains: A CALJET case study and sensitivity to the ENSO cycle. *J. Hydrometeorol.*, **4**, 1243-1264.
- Rigor, I. G., R. L. Colony, and M. Seelye, 2000: Variations in surface air temperature observations in the Arctic, 1979-97. *J. of Climate*, **13** (5), 896-914.
- Rothrock, D. A., Y. Yu, and G. A. Maykut, 1999: Thinning of the Arctic Sea-ice cover, *Geophys. Res. Lett.*, **26**, 3469-3472.
- Rotunno, R., 1983: On the linear theory of the land and sea breeze. *J. Atmos. Sci.*, **40**, 1999-2009.
- SEARCH (Study of Environmental Arctic Change), 2005: *Study of Environmental Arctic Change: Plans for Implementation During the International Polar Year and Beyond*. Fairbanks, Alaska: Arctic Consortium of the United States (ARCUS). 111 pp. [Available at <http://www.arcus.org/SEARCH/index.php>]
- Serreze, M. C., J. A. Maslanik, T. A. Scambos, F. Fetterer, J. Stroeve, K. Knowles, C. Fowler, S. Drobot, R. G. Barry, and T. M. Haran, 2003: A record minimum arctic sea ice extent and area in 2002. *Geophys. Res. Lett.*, **30**(3), 1110, doi:10.1029/2002GL016406.
- Smith, R. B., 1985: On severe downslope winds. *J. Atmos. Sci.*, **42** (23), 2597-2603.

Vinnikov, K. Y, A. Robock, R. J. Stouffer, J. E. Walsh, C. L. Parkinson, D. J. Cavalieri, J. F. B. Mitchell, D. Garrett, and V. F. Zakharov, 1999: Global warming and Northern Hemisphere sea ice extent. *Science*, Washington, DC., **286** (5446), pp. 1934-1937.